# Reconfigurable Phononic-Crystal Circuits Formed by Coupled Acoustoelastic Resonators

Yan-Feng Wang,[1] Ting-Ting Wang,[1] Yue-Sheng Wang,[1,*] and Vincent Laude[2,†]
[1]*Institute of Engineering Mechanics, Beijing Jiaotong University, Beijing 100044, China*
[2]*Institut FEMTO-ST, Université Bourgogne Franche-Comté, CNRS, 25030 Besançon, France*
(Received 17 February 2017; revised manuscript received 8 June 2017; published 10 July 2017)

Reconfigurable phononic circuits can be created by the selective fluid filling of holes in a solid phononic crystal. For frequencies within a complete band gap of the bare phononic crystal, the filled holes become cavities that sustain acoustoelastic defect modes. Those cavities couple evanescently with a strength that depends on their separation. We investigate the dispersion relation and the transmission properties of coupled-resonator acoustoelastic waveguides formed by a chain of cavities. While the dispersion relation is strongly dependent on the separation between cavities, transmission properties are only weakly dependent on the details of the phononic circuit for a fixed separation. Furthermore, depending on the polarization of the source of waves, defect modes can be excited selectively. As a result, rather arbitrary phononic circuits can be created, such as multiply bent waveguides or wave splitters.

DOI: 10.1103/PhysRevApplied.8.014006

## I. INTRODUCTION

Phononic crystals (PCs) are acoustic functional composite materials or structures possessing spatial periodicity [1,2]. They can exhibit elastic or acoustic band gaps in certain frequency ranges, within which wave propagation is prohibited. One significant consequence of such a unique property is the possibility of controlling and manipulating the propagation of acoustic and elastic waves in integrated technological circuits. Consequently, numerous applications of PCs were proposed, such as filtering, multiplexing [3,4], sound isolation [5], frequency-dependent waveguiding [6,7], and mass sensing [8]. An important key to such applications is the confinement and guidance of elastic energy through the use of defects in perfect PCs. Guidance in a sonic or phononic crystal is indeed not limited to linear lines of defects [9]. Using a mechanism based on the coupling of the evanescent fields arising from defect cavities or resonators, rather arbitrary circuits can be defined [10,11], similar to coupled-resonator optical waveguides in photonic crystals [12]. In such waveguides, the dispersion relation is ultimately determined by the coupling strength between resonators, allowing its fine-tuning by varying their separation.

Although PCs provide a promising approach for controlling the propagation of acoustic waves, there are few real-life applications, and experimental realizations of PC-based devices remain scarce. Actually, most PCs are characterized by a passive response and operate in fixed frequency ranges. Topology or material parameters of the fabricated structures are hardly tunable or reconfigurable [13], limiting their possible applications. Tunable manipulation of acoustic or elastic waves has thus become a fast-developing topic. Numerous works have been devoted to the design and development of tunable PCs, for example, by using material [13] or geometric nonlinearities [14]. A similar principle, utilizing magnetoelastic materials [15], was applied to designing a tunable and also reconfigurable solid-solid 2D PC. An external magnetic field was used to change the material properties at will. Such approaches require, however, either magnetoelastic materials or materials with particular nonlinearities.

Reconfigurability can, in principle, be achieved rather easily by using solid-fluid or sonic crystals [16]. Solid-fluid PCs have been considered quite often in the literature, especially in relation to experiments [2]. Different wave equations are used for different regions of space, but they are coupled at the fluid-solid interface [17]. Fluid-solid interaction, for instance, was shown to affect the propagation of acoustic and elastic waves, and even to introduce extra gaps into the band structure [18]. A basic feature of a fluid is that it is shapeless though flowing. This feature makes fluid-solid systems potentially reconfigurable. In other words, acoustic waves in a fluid medium can be manipulated by changing the properties of elastic waves in solid inclusions. Conversely, the propagation of elastic waves in a solid matrix can be controlled through changing the properties of fluid fillings [19,20]. In a solid-fluid PC, fluid filling can thus provide the means for tunability and for reconfigurability. Specifically, fluid-filled holes can confine wave energy to the fluid regions, and thus they behave similarly to defect cavities that can couple via the solid matrix.

In this work, we aim to demonstrate theoretically that coupled-resonator waveguides based on a solid matrix and fluid fillings provide a natural basis for reconfigurable phononic circuits. We first discuss the dispersion relation in

*yswang@bjtu.edu.cn
†vincent.laude@femto-st.fr

 

the case of coupled cavities created by filling holes with liquid in a holey PC presenting a complete band gap. Numerical simulations are performed using the finite-element method. Modal displacements—in the solid matrix—and pressure distribution—in the fluid-filled holes—are presented and are used to discuss the physical mechanism behind waveguiding. Different waveguides are then designed through filling holes to form phononic circuits, and their transmission properties are investigated. It is found that the transmission of wave energy along the circuit is rather independent of its particular shape but strongly depends on the polarization of the source.

## II. DISPERSION RELATIONS

In this section, we discuss the dispersion relation of the coupled-resonator acoustoelastic waveguide (CRAEW). The derivation follows the one for equivalent purely elastic structures [11] but extends it to coupled acoustoelastic wave propagation. Numerical simulations are performed with the finite-element method, taking explicitly into account acoustoelastic coupling [21]. The supercells used in the case of an isolated cavity and in the case of a CRAEW are depicted in Fig. 1. Periodic boundary conditions are applied on pairs of opposite boundaries of the supercell. Phononic band structures are shown in Fig. 2, and some remarkable Bloch waves are displayed in Fig. 3.

For concreteness, we consider isotropic aluminum the solid matrix (mass density $\rho_s = 2700\ \mathrm{kg/m^3}$, Poisson's ratio $\nu = 0.33$, and Young's modulus $E = 68.9$ GPa) and water the fluid that can fill certain holes (mass density $\rho_f = 1000\ \mathrm{kg/m^3}$ and sound velocity $c = 1490\ \mathrm{m/s}$). A two-dimensional square-lattice phononic crystal is chosen for the following examples. The radius $r$ of the hole is set by $r/a = 0.45$, with $a$ being the lattice constant. For this value, a complete band gap is known to appear

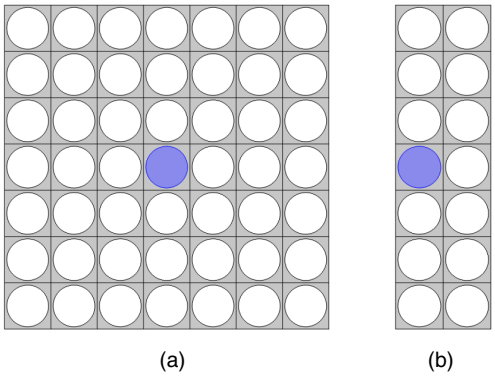


FIG. 1. Supercells used for the calculation of the band structures of (a) a cavity formed by a single point defect in the two-dimensional square-lattice PC and (b) a CRAEW created in the same PC. The blue, gray, and white parts represent water, aluminum, and the vacuum, respectively. The lattice constant, or the distance between adjacent holes, is $a$.

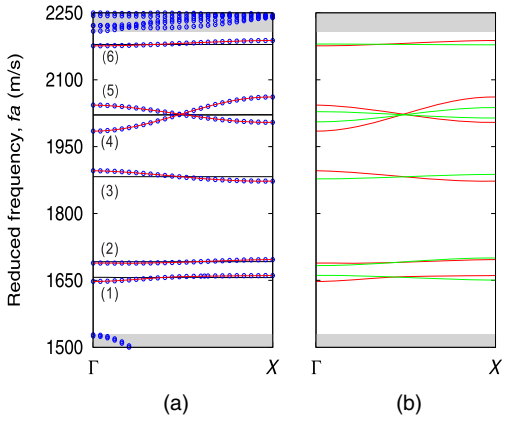


FIG. 2. Dispersion relation for a linear chain of water-filled cavities in a square-lattice phononic crystal of holes in aluminum, forming a CRAEW. (a) Dispersion for cavity separation $\Lambda = 2a$. The result of finite-element computation with the supercell of Fig. 1(b) is shown as blue circles. Horizontal black lines mark the resonant frequencies for the isolated cavity. The gray areas indicate the passing bands for a perfect phononic crystal. The complete band gap extends for $1535\ \mathrm{m/s} < fa < 2206\ \mathrm{m/s}$, with $fa$ being the reduced frequency. The red lines show the CRAEW dispersion relation as obtained with the model of Eq. (1). The dispersion curves are numbered with respect to each defect mode. (b) Comparison of the CRAEW dispersion relation for cavity separation $\Lambda = 2a$ (the red lines) and $\Lambda = 3a$ (the green lines). The fitting coefficients are given in Table I.

for $1535\ \mathrm{m/s} < fa < 2206\ \mathrm{m/s}$, with $f$ being the frequency [22].

The defect modes created by locally filling one hole with water are the basic building blocks of a CRAEW. They can be analyzed with the supercell consisting of $7 \times 7$ circular holes depicted in Fig. 1(a). The size of the supercell is large enough to guarantee that coupling between adjacent defects can be neglected. The resonant frequencies of the six defect modes are listed in Table I. Figure 3 shows the acoustic and elastic polarization of those six defect modes, noted as $S_n$ with $n = 1, 2, \ldots, 6$. Each defect mode has a unique pattern for the distribution of the displacement fields in the solid matrix and of the pressure in the fluid. The displacement fields are such that the amplitude of the vibration decays exponentially away from the defect, thanks to the presence of the complete band gap. Deformations are located mainly at the lumps for modes $S_1$ and $S_2$, and at the thin connectors for modes $S_3$–$S_6$. Modes $S_4$ and $S_5$ are actually frequency degenerate. The different symmetries of the defect modes with respect to the vertical and horizontal axes are listed in Table I. These symmetries are important for understanding the coupling of defect modes with waves incident from the solid matrix.

A CRAEW is formed by considering a sequence of defect cavities separated by a distance $\Lambda$ that is an integral number of lattice constants. When $\Lambda$ is not too large, as shown in Fig. 1(b) for the case $\Lambda = 2a$, the defect modes

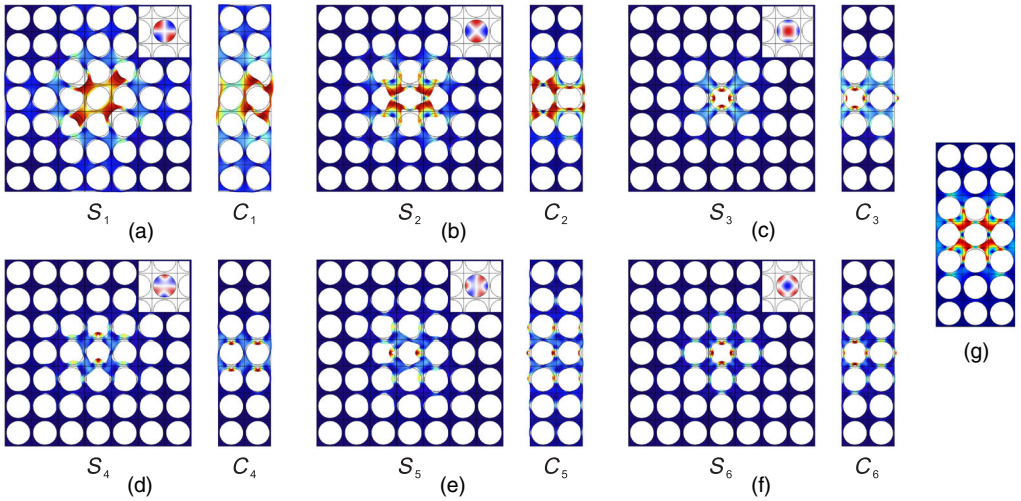


FIG. 3. Displacement and pressure fields of the six defect modes of the acoustoelastic phononic crystal, shown at the Γ point of the first Brillouin zone. (a)–(f) Letters $S_n$ and $C_n$ are for the $n$th defect mode for the isolated cavity and the coupled-resonator waveguides with cavity separation $\Lambda = 2a$, respectively. The pressure distribution in water is shown as an inset in the isolated-cavity case. (g) Displacement field of mode $C_2$ for cavity separation $\Lambda = 3a$.

can couple with each other though the evanescent fields emanating from them. A channel for guided waves can thus be created for frequencies within the complete band gap. The phononic band structure of the CRAEW along the Γ-$X$ direction of the first Brillouin zone is shown in Fig. 2 for the cases $\Lambda = 2a$ and $\Lambda = 3a$. Guided modes are formed around the resonances of the isolated defect with smooth dispersions. The polarizations of those guided Bloch waves at the Γ point, denoted as $C_n$ ($n = 1, 2, \ldots, 6$), are shown in Fig. 3. They are in good correspondence with the corresponding modes of the isolated defect. In other words, wave guidance in a CRAEW comes about owing to the excitation and coupling of similar defect modes.

The dispersion relation of CRAEW modes is very smooth. This property can actually be associated with the rapid decrease with distance of the coupling strength between adjacent cavities, as described by the theoretical model of a linear chain of coupled cavities [11]. The Hamiltonian of the CRAEW is a sum of the Hamiltonians of isolated cavities plus an interaction Hamiltonian describing the interaction of coupled cavities in a quantum treatment [23]. The dispersion can be expressed directly as the Fourier series

$$\omega = \Gamma_0 + \sum_{m=1}^{\infty} 2\Gamma_m \cos(km\Lambda), \tag{1}$$

where $\omega = 2\pi f$ is the angular frequency and $k$ is the wave vector. The Fourier coefficients $\Gamma_m$ can be interpreted as representing the coupling strength between defects separated by a distance $m\Lambda$.

Table I lists the numerical values obtained by fitting the computed CRAEW dispersion relations with Eq. (1). The Fourier series are found to converge very quickly. When compared to the coupling of neighboring cavities for the case of pure shear waves [11], the coupling of fluid cavities in solid PCs remains relatively small. Figure 2(a) compares the dispersion of CRAEW for $\Lambda = 2a$ obtained numerically with the fit in Eq. (1). Numerical and theoretical

TABLE I. Parameters of the dispersion model for linear chains of coupled acoustoelastic cavities. Symmetry ($S$) or antisymmetry ($A$) with respect to the vertical and horizontal axes are given in that order for each of the six defect modes. The third row shows the resonant frequencies of the isolated cavity. Reduced frequencies, $fa$, and expansion coefficients, $\Gamma_m a/(2\pi)$, are given in units of m/s. Expansion coefficients are determined for $\Lambda = 2a$ and $\Lambda = 3a$, and they are obtained by fitting the computed dispersion with the model in Eq. (1).

| | Mode Symmetry | $n = 1$ $AA$ | $n = 2$ $SS$ | $n = 3$ $SS$ | $n = 4$ $SA$ | $n = 5$ $AS$ | $n = 6$ $SS$ |
|---|---|---|---|---|---|---|---|
| Isolated cavity | $fa$ | 1656.77 | 1691.85 | 1882.55 | 2021.08 | 2021.17 | 2179.24 |
| $\Lambda = 2a$ | $\Gamma_0 a/(2\pi)$ | 1656.27 | 1691.68 | 1882.95 | 2023.70 | 2022.68 | 2181.91 |
| | $\Gamma_1 a/(2\pi)$ | −2.95 | −1.96 | 5.80 | −19.15 | 9.57 | −2.93 |
| | $\Gamma_2 a/(2\pi)$ | −1.06 | 0.49 | 0.64 | −0.29 | 0.58 | 0.072 |
| | $\Gamma_3 a/(2\pi)$ | −0.34 | 0.02 | 0.04 | 0.01 | 0.10 | −0.05 |
| $\Lambda = 3a$ | $\Gamma_0 a/(2\pi)$ | 1656.31 | 1691.74 | 1882.58 | 2021.78 | 2021.26 | 2179.29 |
| | $\Gamma_1 a/(2\pi)$ | 2.58 | −4.29 | −2.46 | −7.96 | 3.51 | 0.41 |
| | $\Gamma_2 a/(2\pi)$ | −0.20 | −0.03 | 0.07 | −0.07 | 0.05 | 0.00 |
| | $\Gamma_3 a/(2\pi)$ | 0.02 | 0.00 | −0.00 | −0.00 | 0.00 | −0.00 |

results match very well with only the first four Fourier coefficients considered, meaning that couplings need only be considered up to the third-nearest-neighboring cavity. If the separation between cavities is increased to $\Lambda = 3a$, the dispersion generally gets even smaller, as shown in Fig. 2(b). The fitted Fourier coefficients are listed in Table I in this case also. Except for the particular case of mode $S_2$, the Fourier coefficients are generally smaller compared to the case $\Lambda = 2a$. The polarization of mode $S_2$ at the $\Gamma$ point is shown in Fig. 3(g) for $\Lambda = 3a$ for the sake of completeness.

The results in this section suggest the possibility of creating reconfigurable phononic circuits based on CRAEWs. Indeed, different CRAEWs can be designed based on the coefficients listed in Table I. In the following, we will specifically consider the case $\Lambda = 2a$ for the design of phononic circuits. Similar results and conclusions would be obtained for larger separations, such as $\Lambda = 3a$. It should be noted that, for line-defect waveguides formed when $\Lambda = a$, the guiding mechanism is different [2,9]. Specifically, the interaction between different guiding bands would be much stronger and would lead to their interference and the opening of mini–band gaps for guided waves. The guided bands considered in this paper are isolated so that the circuits support single-mode guided propagation.

## III. PHONONIC CIRCUITS

In this section, we consider phononic circuits created by filling with a fluid certain holes of a solid phononic crystal. Computations are performed for a finite phononic crystal with $19 \times 19$ primitive cells, as shown in Fig. 4. Phononic circuits are characterized by the transmission of waves through them. We first consider different variations on the theme of the coupled-resonator acoustoelastic waveguide, with or without bends, before moving on to a simple wave splitter.

Figure 4 depicts three different waveguides for which fluid-filled cavities are separated by the distance $\Lambda = 2a$. The fluid cavities are distributed in three different circuits: (a) a straight circuit formed by a sequence of ten cavities, (b) a circuit formed by a sequence of 13 cavities with two bends, and (c) a circuit formed by a sequence of 17 cavities with eight bends. In the following, we refer to them as the straight waveguide, the two-bend waveguide, and the eight-bend waveguide, respectively.

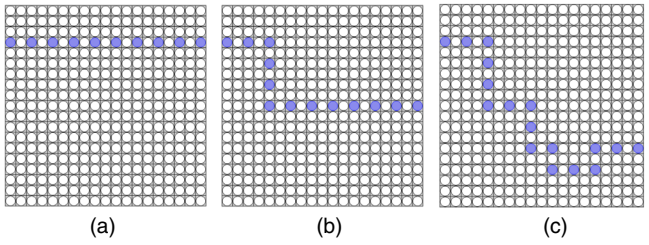


FIG. 4. Cross sections of coupled-resonator acoustoelastic waveguides formed by filling holes with water in different circuits on a finite phononic crystal with $19 \times 19$ cells. (a) Straight waveguide. (b) Two-bend waveguide. (c) Eight-bend waveguide.

Transmission through a circuit is estimated as follows. A line source for elastic waves polarized along either the $x$ axis (longitudinal excitation) or the $y$ axis (shear excitation) is positioned along segment $S_l$ at the left side of the waveguide. Excitation along the $z$ axis is not considered, as vertical shear waves in the solid do not couple to pressure waves in the fluid for the two-dimensional case considered here. The length of the source segment $S_l$ is exactly one lattice constant $a$. The amplitude of the displacement at the line source is noted $U_0$. Low-reflection boundary conditions are applied on all other external boundaries of the computation domain. By sweeping the reduced frequency, we evaluate the transmission $T(fa)$ in decibel units by

$$T(fa) = 20\log_{10}\left(\frac{\int_{S_r} U ds}{\int_{S_l} U_0 ds}\right), \tag{2}$$

where $U$ is the total displacement along $S_r$, a receiver segment placed at the right exit of the waveguide. Instead of displacement, it would be perfectly possible to compute the flux of the Poynting vector at input and exit boundaries. This flux, however, would be a superposition of right- and left-traveling guided waves, owing to the remaining small reflections at the boundaries, so the result would not simply represent directional energy-flux propagation. Nevertheless, all transmissions in this paper respect the principle of conservation of energy.

The transmissions for the different waveguides are shown in Fig. 5 as a function of reduced frequency. Five passing frequency ranges, labeled I–V in the figure, are clearly observed inside the complete band gap. These passing frequency ranges coincide with the CRAEW dispersion bands in Fig. 2(a): Range I can be identified with the band for Bloch wave $C_1$, II with $C_2$, III with $C_3$, and V with $C_6$. Range IV can be identified with a mixture of Bloch waves $C_4$ and $C_5$, as we will argue later. It is apparent that there are no significant differences in the extent of passing frequency ranges for different circuits, though the precise oscillations inside the passing bands are characteristic of each circuit. These oscillations are caused by the interference of waves traveling along the waveguide and depend on its total length. For frequencies between passing bands, transmission is generally very low but again depends on the total length of the waveguide: the longer the coupled-resonator waveguide, the smaller the transmission. These results indicate that rather arbitrary waveguides can be defined based on the CRAEW principle, i.e., waveguides with arbitrary bends.

Comparing transmissions in Fig. 5, we find that passing frequency ranges II, III, and V are dominantly excited by

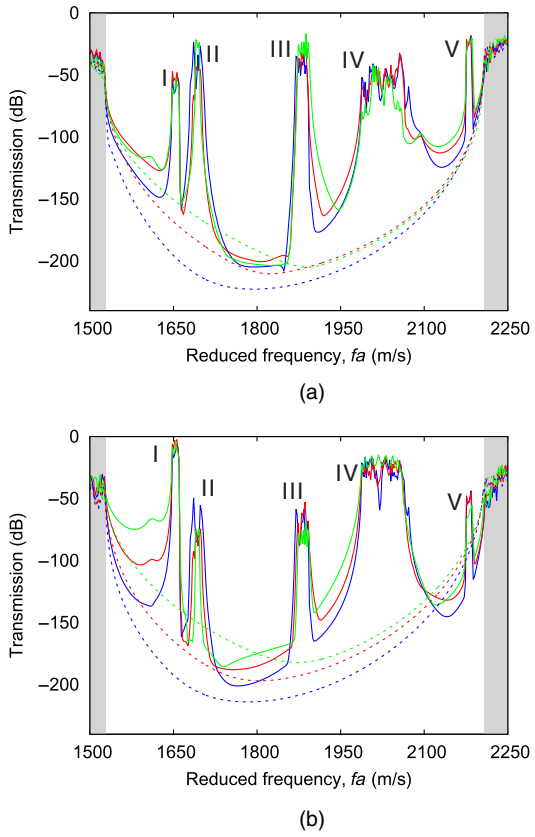


FIG. 5. Transmission as a function of frequency through the coupled-resonator acoustoelastic waveguides of Fig. 4 for (a) a longitudinal wave source and (b) a shear wave source. Transmission is shown for the straight waveguide (the green line), the two-bend waveguide (the red line), and the eight-bend waveguide (the blue line). I–V represent the five passing frequency ranges. For comparison, transmission through the bare phononic crystal is also plotted with dashed lines, with source and receiver positioned as in the case of waveguides.

the wave source of longitudinal polarization, while ranges I and IV are dominantly excited by the wave source of shear polarization. Animations of the pressure distribution along the eight-bend waveguide as a function of frequency and polarization of the source can be viewed in Videos 1 and 2 for a lattice constant $a = 20$ mm. The pressure distribution along the eight-bend waveguide is shown in Fig. 6(a) at $fa = 1882$ m/s (range III) for longitudinal excitation and in Fig. 6(b) at $fa = 2004$ m/s (range IV) for shear excitation. Pressure patterns similar to Bloch waves $S_3$, and to a mixture of Bloch waves $S_4$ and $S_5$, respectively, are clearly observed. As Bloch waves $S_4$ and $S_5$ are of orthogonal polarization, there is a superposition of two independent transmission channels in the common frequency range of bands $C_4$ and $C_5$ in Fig. 2(a). These results suggest that the different defect modes can be independently generated and controlled by selecting excitation frequencies and polarization. As a perspective, it seems also likely that wave sources perfectly adapted to each

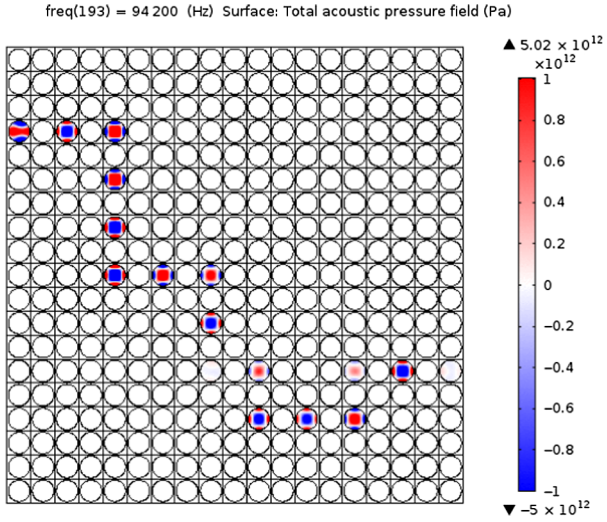


VIDEO 1. Animation of the pressure distribution along the eight-bend waveguide as a function of frequency for a longitudinal wave source.

defect mode could be defined. In the case of perfect adaptation, unit transmission from the source to the last cavity might be achievable. Obviously, the wave sources that we consider, having uniform displacement amplitude along the straight boundary $S_l$, are not optimal in this respect.

Transmission for the bare phononic crystal, i.e., that without any filled cavity, is added to Fig. 5 for comparison. It is found that the transmission for waveguides can be smaller than for the bare crystal, especially in the case of the shear wave source. This observation can be explained using the complex band structure [24] in comparison with the transmission [25]. We have verified that the complex band structure is significantly modified for certain

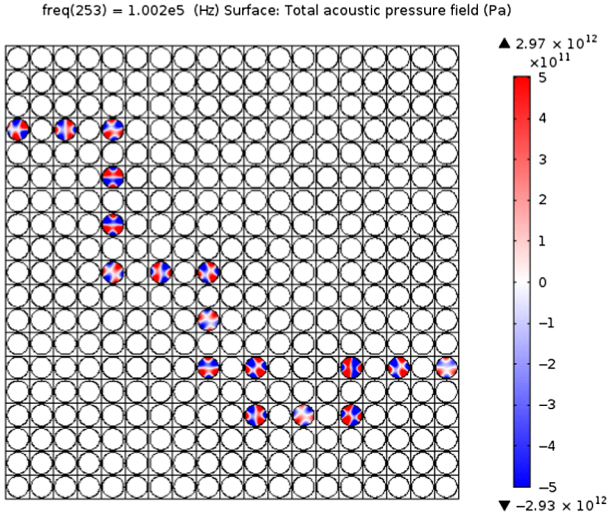


VIDEO 2. Animation of the pressure distribution along the eight-bend waveguide as a function of frequency for a shear wave source.

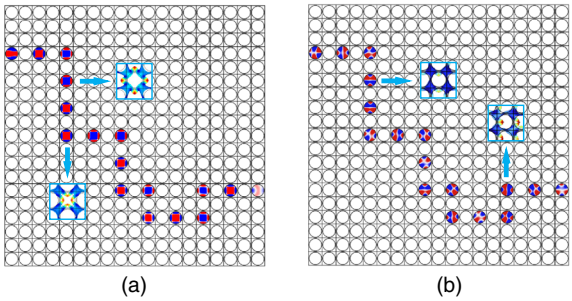


FIG. 6. Normalized pressure distribution for (a) a longitudinal wave source at the reduced frequency $fa = 1883$ m/s and (b) a shear wave source at $fa = 2004$ m/s. The color scale goes from negative (blue) to positive (red). (Insets) Displacements around selected cavities.

frequencies when certain hollow cavities are filled with water. For example, the smallest imaginary part, which plays a dominant role in the determination of the attenuation inside a Bragg band gap [26], undergoes fast changes as a function of frequency and polarization.

When different defects are combined, it is known that various acoustic devices can be designed, such as the acoustic wave splitter [27]. Here, based on the CRAEW principle, the design of the elastic wave splitter illustrated in Fig. 7 is discussed. The phononic circuit is composed of one straight part and two asymmetric bent parts with different lengths. A wave source of longitudinal vibrations is placed at the left side of the waveguide. Elastic waves first propagate along the straight part, and they are then evenly split into the two bent waveguides. An animation of the pressure distribution along the wave splitter as a function of frequency can be viewed in Video 3 for a lattice

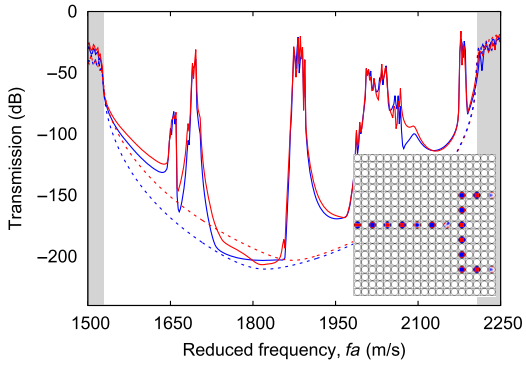


FIG. 7. Transmission as a function of frequency through a wave splitter composed of a straight waveguide separating into two bent waveguides for a longitudinal wave source. Transmissions at the end of the upper (red line) and lower (blue line) bent waveguides are displayed. (Inset) The normalized pressure distribution at reduced frequency $fa = 1882$ m/s. The color scale goes from negative (blue) to positive (red). For comparison, transmission through the bare phononic crystal is also plotted with dashed lines, with the source and the receiver positioned as in the case of the splitter circuit.

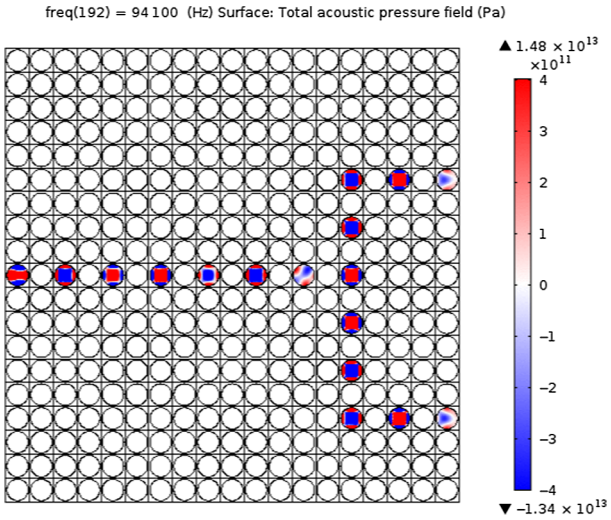


VIDEO 3. Animation of the pressure distribution along the wave splitter as a function of frequency for a longitudinal wave source.

constant $a = 20$ mm. The wave-splitting function is illustrated in the inset of Fig. 7 by the pressure distribution at reduced frequency $fa = 1882$ m/s. Similar to the results obtained for different circuits in Fig. 5, the transmissions measured at the two ends of the splitter are almost the same in the passing frequency ranges, and slightly different outside of them owing to different circuit lengths. The splitter circuit ensures that wave amplitude is equally split at the junction. However, the outputs at the two ends may differ slightly in amplitude because the lengths of the two waveguides following the splitter are unequal: reflections at the ends hence interfere with incoming waves with different phases. It is worthwhile noting that this difference would disappear if there were no reflection at the ends. Reciprocally, it can be noted that if different signals of the same frequency were sent from the ends of the splitter, they would be combined into the straight waveguide.

Before concluding the paper, let us discuss some practical aspects of phononic circuits composed of CRAEWs. First, we consider two-dimensional infinite phononic crystals, but the idea can be extended straightforwardly to two-dimensional phononic crystal slabs. The main effect we can expect is a reduction of the width of the complete band gap and its dependence on the slab thickness. Furthermore, the independence of in-plane and out-of-plane polarized waves would be lost. Second, the domain of application is typically dependent on the lattice-constant value. On the theoretical side, all band structures and transmission spectra simply scale with the lattice constant as indicated by the reduced-frequency definition, at least for lossless materials. In practice, however, transmission through a circuit is sensitive to acoustic wave damping in the fluid-filled holes. The viscosity of water is frequency dependent and can be accounted for using a viscous-fluid model [28]. With damping taken into

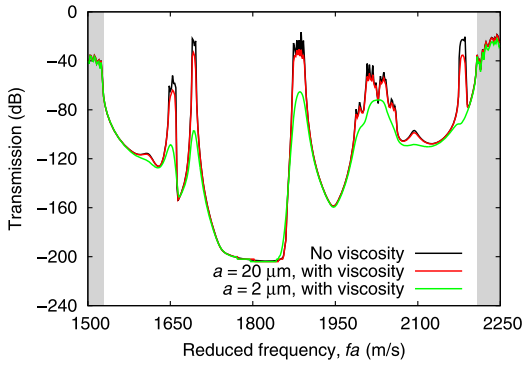


FIG. 8. Influence of viscous damping in water on the transmission spectrum of the straight coupled-resonator acoustoelastic waveguide of Fig. 4(a), for a longitudinal wave source.

account, the transmission spectrum depends on the lattice constant $a$, as shown in Fig. 8 for the case of the straight waveguide. It is seen that damping has a limited influence on transmission for lattice constants larger than 20 $\mu$m. For smaller lattice constants, e.g., in micron-scale phononic circuits, viscous damping increases rapidly. It can be further remarked that viscous damping is more pronounced in passing frequency ranges than outside of them. This is readily explained by observing that guided waves in CRAEWs have a very flat dispersion, corresponding to small group velocities. Indeed, it is known that spatial decay on propagation is proportional to intrinsic material loss and inversely proportional to the group velocity [29].

In this paper, we observe that damping in water introduces a frequency dependence that becomes relevant at a small scale, typically when $a < 20$ $\mu$m. This result implies that the phononic circuits we describe could operate from small frequencies up to about 100 MHz, covering the typical range of ultrasonic applications, such as medical ultrasound, nondestructive evaluation, etc. Selective fluid filling of holes is a technical problem that can be tackled in different mechanical or chemical ways, depending on the hole size. Spotting machines can, for instance, be used to form picoliter-volume droplets and infiltrate them into individual holes with diameters on the order of 10 $\mu$m. Furthermore, techniques that have been developed in the field of optofluidics to infiltrate submicron holes in photonic crystal devices [30,31] could also be applied to reconfiguring phononic circuits.

## IV. CONCLUSIONS

In this paper, coupled acoustoelastic wave propagation in circuits formed by evanescent coupling of chains of defect cavities is studied. Defect cavities are introduced by filling a number of selected holes with a liquid in a two-dimensional square-lattice PC composed of periodic circular holes in a solid matrix. The localized defect modes appearing inside the complete band gap of the perfect PC are the building blocks of a CRAEW. The consideration of fluid filling naturally confers reconfigurability to the circuits and reusability of the solid matrix. Reciprocally, the solid matrix, in which the phononic circuit is defined, ensures its durability and stability.

When a linear chain of such defect cavities is constructed, evanescent coupling of the cavities gives rise to guided modes that are finely confined along the chain and whose dispersion relation can be tuned by varying the separation between defects and, ultimately, by varying the acoustic properties of the fluid, though only water is considered in this paper. Different waveguides with up to eight bends are considered and it is found that transmission of well-confined waves is achieved, regardless of the details of the circuits. Outside passing frequency ranges, transmission though circuits may even be smaller than through the bare PC, owing to the generation of evanescent waves originating from defect cavities. As an example of a potential wave device, a 50:50 wave splitter is designed based on the combination of different CRAEWs. Finally, transmission damping arising from fluid viscosity is estimated as a function of the lattice constant.

This work provides prospects for reconfigurable and tunable manipulation of acoustoelastic wave propagation. Consideration of more complex phononic circuits than those examined in this paper is straightforward basing on the CRAEW concept. By using different kinds of fluids or by using a fluid whose properties can be tuned by external means, the phononic circuit could, furthermore, be made tunable. Active—or even smart—manipulation of elastic waves could be achieved.

## ACKNOWLEDGMENTS

Financial support by the National Natural Science Foundation of China (Grants No. 11642023 and No. 11532001) is gratefully acknowledged. Y.-F. W. acknowledges the support of Fundamental Research Funds for the Central Universities (Grant No. 2016RC042). V. L. acknowledges the financial support of the Labex ACTION program (Contract No. ANR-11-LABX-0001-01).

[1] M. S. Kushwaha, P. Halevi, L. Dobrzynski, and B. Djafari-Rouhani, Acoustic Band Structure of Periodic Elastic Composites, Phys. Rev. Lett. **71**, 2022 (1993).

[2] V. Laude, *Phononic Crystals: Artificial Crystals for Sonic, Acoustic, and Elastic Waves* (Walter de Gruyter GmbH, Berlin, 2015).

[3] S. Bringuier, N. Swinteck, J. O. Vasseur, J.-F. Robillard, K. Runge, K. Muralidharan, and P. A. Deymier, Phase-controlling phononic crystals: Realization of acoustic Boolean logic gates, J. Acoust. Soc. Am. **130**, 1919 (2011).

[4] N. Swinteck, J. O. Vasseur, A.-C. Hladky-Hennion, C. Croënne, S. Bringuier, and P. A. Deymier, Multifunctional solid/solid phononic crystal, J. Appl. Phys. **112**, 024514 (2012).

[5] T.-T. Wu, W.-S. Wang, J.-H. Sun, J.-C. Hsu, and Y.-Y. Chen, Utilization of phononic-crystal reflective gratings in a layered surface acoustic wave device, Appl. Phys. Lett. **94**, 101913 (2009).
[6] P. H. Otsuka, K. Nanri, O. Matsuda, M. Tomoda, D. M. Profunser, I. A. Veres, S. Danworaphong, A. Khelif, S. Benchabane, and V. Laude, Broadband evolution of phononic-crystal-waveguide eigenstates in real- and *k*-spaces, Sci. Rep. **3**, 3351 (2013).
[7] F.-L. Hsiao, A. Khelif, H. Moubchir, A. Choujaa, C.-C. Chen, and V. Laude, Waveguiding inside the complete band gap of a phononic crystal slab, Phys. Rev. E **76**, 056601 (2007).
[8] D. Nardi, E. Zagato, G. Ferrini, C. Giannetti, and F. Banfi, Design of a surface acoustic wave mass sensor in the 100 GHz range, Appl. Phys. Lett. **100**, 253106 (2012).
[9] A. Khelif, A. Choujaa, S. Benchabane, B. Djafari-Rouhani, and V. Laude, Guiding and bending of acoustic waves in highly confined phononic crystal waveguides, Appl. Phys. Lett. **84**, 4400 (2004).
[10] R. Sainidou, N. Stefanou, and A. Modinos, Linear chain of weakly coupled defects in a three-dimensional phononic crystal: A model acoustic waveguide, Phys. Rev. B **74**, 172302 (2006).
[11] J. M. Escalante, A. Martínez, and V. Laude, Dispersion relation of coupled-resonator acoustic waveguides formed by defect cavities in a phononic crystal, J. Phys. D **46**, 475301 (2013).
[12] A. Yariv, Y. Xu, R. K. Lee, and A. Scherer, Coupled-resonator optical waveguide: A proposal and analysis, Opt. Lett. **24**, 711 (1999).
[13] K. L. Manktelow, M. J. Leamy, and M. Ruzzene, Topology design and optimization of nonlinear periodic materials, J. Mech. Phys. Solids **61**, 2433 (2013).
[14] P. Wang, J. Shim, and K. Bertoldi, Effects of geometric and material nonlinearities on tunable band gaps and low-frequency directionality of phononic crystals, Phys. Rev. B **88**, 014304 (2013).
[15] J. O. Vasseur, O. Bou Matar, J.-F. Robillard, A.-C. Hladky-Hennion, and P. A. Deymier, Band structures tunability of bulk 2D phononic crystals made of magneto-elastic materials, AIP Adv. **1**, 041904 (2011).
[16] M. Caleap and B. W. Drinkwater, Acoustically trapped colloidal crystals that are reconfigurable in real time, Proc. Natl. Acad. Sci. U.S.A. **111**, 6226 (2014).
[17] J.-B. Li, Y.-S. Wang, and C. Zhang, Dispersion relations of a periodic array of fluid-filled holes embedded in an elastic solid, J. Comput. Acoust. **20**, 1250014 (2012).
[18] J. S. Jensen and J. Kook, Coupled acoustic-mechanical bandgaps, Crystals **6**, 112 (2016).
[19] F. Casadei and K. Bertoldi, Harnessing fluid-structure interactions to design self-regulating acoustic metamaterials, J. Appl. Phys. **115**, 034907 (2014).
[20] Y. Jin, Y. Pennec, Y. Pan, and B. Djafari-Rouhani, Phononic crystal plate with hollow pillars actively controlled by fluid filling, Crystals **6**, 64 (2016).
[21] R. P. Moiseyenko, N. F. Declercq, and V. Laude, Guided wave propagation along the surface of a one-dimensional solid-fluid phononic crystal, J. Phys. D **46**, 365305 (2013).
[22] Y.-F. Wang, Y.-S. Wang, and X.-X. Su, Large bandgaps of two-dimensional phononic crystals with cross-like holes, J. Appl. Phys. **110**, 113520 (2011).
[23] F. M. Hu, L. Zhou, T. Shi, and C. P. Sun, Coupled cavity QED for coherent control of photon transmission: Green-function approach for hybrid systems with two-level doping, Phys. Rev. A **76**, 013819 (2007).
[24] V. Laude, Y. Achaoui, S. Benchabane, and A. Khelif, Evanescent Bloch waves and the complex band structure of phononic crystals, Phys. Rev. B **80**, 092301 (2009).
[25] Y.-F. Wang, Y.-S. Wang, and V. Laude, Wave propagation in two-dimensional viscoelastic metamaterials, Phys. Rev. B **92**, 104110 (2015).
[26] V. Romero-García, J. V. Sánchez-Pérez, S. Castineira-Ibánez, and L. M. Garcia-Raffi, Evidences of evanescent Bloch waves in phononic crystals, Appl. Phys. Lett. **96**, 124102 (2010).
[27] Y. Pennec, B. Djafari-Rouhani, J. O. Vasseur, A. Khelif, and P. A. Deymier, Tunable filtering and demultiplexing in phononic crystals with hollow cylinders, Phys. Rev. E **69**, 046608 (2004).
[28] S. Temkin, *Elements of Acoustics* (Acoustical Society of America, West Barnstable, MA, 2001).
[29] V. Laude, J. M. Escalante, and A. Martínez, Effect of loss on the dispersion relation of photonic and phononic crystals, Phys. Rev. B **88**, 224302 (2013).
[30] C. Monat, P. Domachuk, and B. J. Eggleton, Integrated optofluidics: A new river of light, Nat. Photonics **1**, 106 (2007).
[31] A. C. Bedoya, P. Domachuk, C. Grillet, C. Monat, E. C. Mägi, E. Li, and B. J. Eggleton, Reconfigurable photonic crystal waveguides created by selective liquid infiltration, Opt. Express **20**, 11046 (2012).